J. Fluid Mech. (1983), *vol.* 132, *pp.* 119–144
Printed in Great Britain

Instabilities of dynamic thermocapillary liquid layers. Part 1. Convective instabilities

By MARC K. SMITH† AND STEPHEN H. DAVIS

Department of Engineering Sciences and Applied Mathematics, The Technological Institute, Northwestern University, Evanston, Illinois 60201

(Received 7 October 1982 and in revised form 18 January 1983)

A planar liquid layer is bounded below by a rigid plate and above by an interface with a passive gas. A steady shear flow is set up by imposing a temperature gradient along the layer and driving the motion by thermocapillarity. This dynamic state is susceptible to two types of thermal-convective instabilities: (i) stationary longitudinal rolls, which involve the classical Marangoni instability studied by Pearson; and (ii) unsteady hydrothermal waves, which involve a new mechanism of instability deriving its energy from the horizontal temperature gradients. Thermal stability characteristics for liquid layers with and without return-flow profiles are presented as functions of the Prandtl number of the liquid and the Biot number of the interface. Comparisons are made with available experimental observations.

1. Introduction

The surface tension of an interface between two immiscible fluids is generally a monotonically decreasing function of temperature. Unless opposed by effects of contamination, say, any temperature gradient imposed *along* the interface will produce a corresponding gradient in surface tension and hence a bulk fluid motion. This type of motion is called thermocapillary or Marangoni convection.

There are many physical systems involving heat and/or mass transfer across interfaces in which thermocapillary convection has an important or even a dominant effect. Among them are the migration of a droplet or a bubble in a non-uniform temperature field (Young, Goldstein & Block 1959; Papazian, Gutowski & Wilcox 1979, Subramanian 1981), flame spreading over pools of liquid fuel (Sirignano 1972), and the extinction of a burning wick in a shallow layer of fuel (Adler 1970). Complete reviews of physical processes where surface-tension gradients are important are given by Scriven & Sternling (1960) and by Kenning (1968).

Our particular interest involves the floating-zone process of bulk crystal growth from the melt. This technique is containerless so that the melt cannot pick up additional impurities from a melt container. As shown in figure 1(*a*), feed material is fed upwards through a ring heater and only a small zone of the material near the heater is melted. As the upper rod moves upward, the melt recrystallizes at the melt–crystal interface to form a single crystal. In Earth-based applications, the size of the zone must be small enough so that capillary forces can contain the melt between the crystal and the feed against the force of gravity. Somewhat larger melt zones may

† Present address: Department of Mathematics, Massachusetts Institute of Technology, Cambridge, Massachusetts 02139.

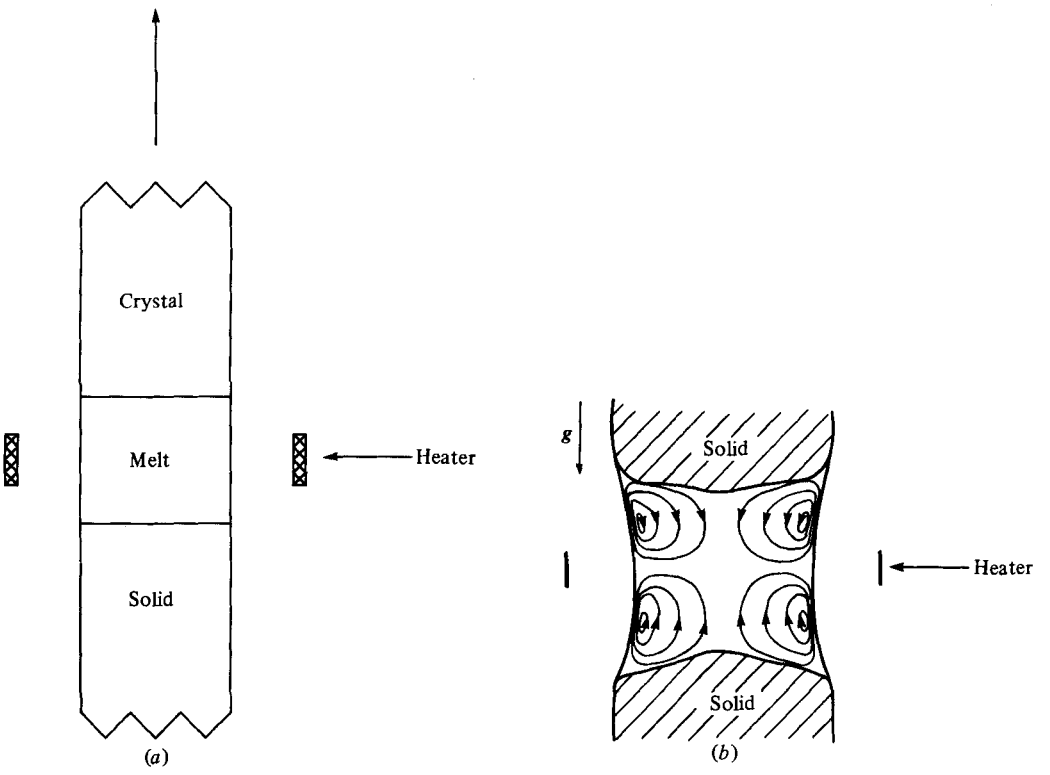

FIGURE 1. Sketches of (*a*) the geometry of the floating-zone crystal growth techniques; and (*b*) the typical thermocapillary convection cells seen in a floating zone, after Schwabe *et al.* (1978).

be obtained in the microgravity environment of Space. For these reasons the floating-zone technique is deemed important in the processing of single crystals in Space.

The existence and magnitude of thermocapillary convection cells in the melt of the floating-zone process (shown in figure 1*b*) has been demonstrated experimentally by Schwabe *et al.* (1978) and by Chun & Wuest (1978*a*). Numerical simulations of this motion have been produced by among others Chun & Wuest (1978*b*) and Clark & Wilcox (1980). All these results have shown that thermocapillary motion will assume a dominant role in the heat and mass transfer that occurs in the floating-zone process in Space and even in some terrestrial applications.

In crystal growth from the melt, the final product is, hopefully, a high-quality single crystal with uniform material properties. One of the problems associated with these processing techniques is the development of striations or segregation bands parallel to the melt–crystal interface. These striations are regions of varying impurity concentration which result in a non-uniform material property distribution in the final product. The underlying cause of these striations seems to be a time-dependent crystal-growth speed brought about by temperature oscillations in the melt.

One origin of these temperature oscillations is an instability in the flow field of the melt (Wilcox 1971). In terrestrial applications, buoyancy forces can drive the instability (Carruthers 1976). However, in the near-absence of gravity an instability of the basic thermocapillary flow may cause the observed temperature oscillations.

Schwabe & Scharmann (1979) demonstrated experimentally the existence of a thermocapillary instability in small floating half-zones. For a given zone geometry, time-dependent temperature and velocity perturbations were observed in the melt

when the temperature drop across the half-zone exceeded a well-defined critical value. Above this critical value the oscillations possessed a well-defined frequency. In a similar series of experiments, Chun & Wuest (1979) also demonstrated the existence of such an instability. In fact, the critical dimensionless number used to measure the temperature drop across the zone, i.e. the Marangoni number, is nearly the same in both sets of experiments. Kölker (1980) also observed an instability and the resulting crystal striations in a silicon melt with a free surface. He concluded that buoyancy could not drive the instability but that thermocapillary forces could.

The theoretical development of thermocapillary instabilities has been limited so far to static liquid layers heated from below. Pearson (1958) was the first to describe the onset of Marangoni convection in this geometry. If a temperature gradient is applied perpendicular to the free surface, there can be a purely conductive basic state in which the fluid is motionless. Pearson studied the instability of this ideal state. However, in most common physical situations the imposed temperature gradient will have a component *parallel* to the free surface so that interfacial motions are generated. The resulting basic state is dynamic, not static; it involves axial convection and a shear flow in the bulk. Indeed, in the physical examples discussed previously, the temperature gradient is directed primarily *along* the interface. The instability of this dynamic basic state has not yet been considered.

We begin this investigation by considering thermocapillary flows in two simple, planar geometries: an infinite, horizontal liquid layer and a liquid layer in a thin two-dimensional slot. Each layer is set into motion by a temperature gradient imposed *along* its free surface.

Through our consideration of these flow fields we have identified two broad classes of instabilities. The first is a convective or thermal instability, whose mechanism involves a balance between heat conduction and heat convection at the free surface. This balance is relatively unaffected by free-surface deformation. The second class is a surface-wave instability, whose mechanism involves the mechanical transfer of momentum from the basic state to the disturbances through the Reynolds stress in the layer. Free-surface deformation is vitally important to this second stability. In the present paper we shall investigate the thermal instabilities and leave the surface-wave instabilities to the companion paper (Smith & Davis 1983).

Since free-surface deformation has a relatively small effect on the thermal instability, we shall follow Pearson (1958) and simplify the analysis by limiting ourselves to a non-deformable free surface. The thermal instabilities that result are of two types. The first takes the form of *stationary longitudinal rolls* that become unstable in much the same way as the classical Marangoni layer heated from below. However, these rolls do interact with the underlying shear flow. The energy driving the instability comes from the *vertical* temperature gradient induced by a balance between horizontal convection and vertical conduction. These rolls can exist at large Prandtl numbers.

The second thermal instability takes the form of *propagating hydrothermal waves*. These waves derive their energy from the imposed *horizontal* temperature gradient when the Prandtl number of the liquid is small and from the *vertical* temperature gradient when the Prandtl number is large. This new mechanism of instability in dynamic basic states is explained in detail.

The thermal-stability characteristics for each layer are calculated and related to the Prandtl number of the liquid and to the Biot number of the interface. Relevant experiments are discussed and the calculated results are compared with observation.

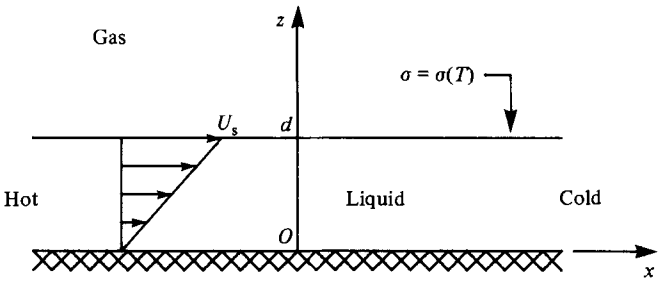

FIGURE 2. A sketch of the geometry of the infinite, horizontal liquid layer. A constant temperature gradient imposed along the layer gives rise to the indicated basic-state velocity profile.

2. The three-dimensional disturbance equations

2.1. *The mathematical model*

Consider a liquid layer of infinite horizontal extent bounded by a rigid plane at $z = 0$ and a free surface having mean position at $z = d$. The origin of the Cartesian coordinate system used lies in the rigid plane and the z-axis points normal to this plane into the liquid. The layer, shown in figure 2, is composed of an incompressible Newtonian liquid with constant viscosity μ, density ρ, specific heat c_p, thermal conductivity k and unit thermal surface conductance h. The surface tension σ of the interface varies with the temperature T of the liquid. A constant temperature gradient $\mathrm{d}T/\mathrm{d}x = -b$, $b > 0$, is imposed *along* the layer. There are no body forces.

The equation of state for the surface tension is approximated by

$$\sigma = \sigma_0 - \gamma(T - T_0), \tag{2.1}$$

where T_0 is the temperature of the interface at $x = 0$, say, σ_0 is the surface tension at this temperature, and $\gamma = -\mathrm{d}\sigma/\mathrm{d}T > 0$ is the negative rate of change of surface tension with temperature.

We consider the fully three-dimensional system and scale all distances on the average liquid depth d. The velocity vector $\boldsymbol{v} = (u, v, w)$, pressure p, temperature difference $T - T_0$, surface tension σ and time t are referred to scales $\gamma bd/\mu$, γb, bd, σ_0 and $\mu/\gamma b$ respectively. As a result, there arise the following dimensionless groups:

$$R \equiv \frac{\rho\gamma bd^2}{\mu^2}, \quad Pr \equiv \frac{\mu c_p}{k}, \quad B \equiv \frac{hd}{k}, \quad S \equiv \frac{\rho d\sigma_0}{\mu^2}. \tag{2.2a, b, c, d}$$

R is the Reynolds number, Pr is the Prandtl number, B is the surface Biot number and S is the non-dimensional surface-tension number. Another useful dimensionless group is the Marangoni number, defined as

$$M \equiv RPr. \tag{2.2e}$$

In general, the free surface is located at $z = 1 + \eta(x, y, t)$, where the mean value of $\eta(x, y, t)$ is zero. However, we consider the limit of $S \to \infty$ in which the free surface of the liquid layer becomes a planar, non-deformable interface with thermocapillary shear stresses in the surface balanced by bulk shear stresses (Davis & Homsy 1980).

In this case the mechanical boundary conditions at the free surface can be expressed as follows:

$$w = 0, \tag{2.3a}$$

$$\frac{\partial u}{\partial z} = -\frac{\partial T}{\partial x}, \tag{2.3b}$$

$$\frac{\partial v}{\partial z} = -\frac{\partial T}{\partial y}. \tag{2.3c}$$

We assume that the bounding gas is passive, with a constant pressure taken equal to zero.

The equality of heat flux at the free surface between the layer and the bounding gas requires that

$$-\frac{\partial T}{\partial z} = B(T-T_\infty)+Q \quad \text{on} \quad z = 1. \tag{2.3d}$$

Here T_∞ is the temperature of the bounding gas far from the interface and Q is an imposed heat flux to the surrounding environment which is determined by the particular basic-state solution under consideration. Note that Q is not an independent parameter.

On the rigid lower plane there is no slip and zero heat flux:

$$u = v = w = \frac{\partial T}{\partial z} = 0 \quad \text{on} \quad z = 1. \tag{2.4}$$

The governing equations for the liquid layer are the Navier–Stokes equations, the energy equation and the continuity equation:

$$R\left[\frac{\partial v_i}{\partial t} + v_j v_{i,j}\right] = -p_{,i} + \nabla^2 v_i, \tag{2.5a}$$

$$M\left[\frac{\partial T}{\partial t} + v_i T_{,i}\right] = \nabla^2 T, \tag{2.5b}$$

$$v_{i,i} = 0. \tag{2.5c}$$

where the summation convention is used over the range $i = 1, 2, 3$.

2.2. *The basic states*

We consider two parallel-flow solutions to the system (2.3)–(2.5). The first, which we refer to as the *linear-flow solution*, is defined as follows:

$$\bar{v} = (\bar{u}, \bar{v}, \bar{w}) = (z, 0, 0), \tag{2.6a}$$

$$\bar{p} = 0, \tag{2.6b}$$

$$\bar{T} = -x + \tfrac{1}{6}M(1-z^3), \tag{2.6c}$$

$$\bar{T}_\infty = -x, \tag{2.6d}$$

$$\bar{Q} = \tfrac{1}{2}M. \tag{2.6e}$$

The layer has a flat top and an x-component of velocity which is linear in z (i.e. plane Couette flow). The temperature field is linear in x as imposed, plus a distribution in z obtained from a balance between vertical conduction and horizontal convection. We term this latter temperature distribution the *flow-induced temperature field*. Here

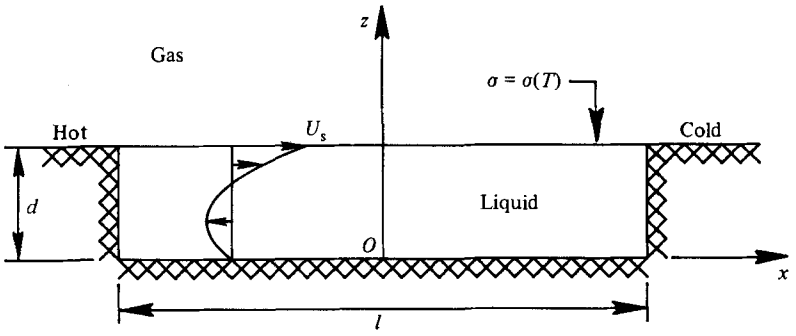

FIGURE 3. A sketch of the geometry of the two-dimensional slot. If $d/l \ll 1$ then a constant temperature gradient imposed along the layer can give rise to the indicated approximate basic-state velocity profile.

the flow-induced temperature field makes the fluid at the lower plate warmer than that at the interface.

The second solution, which we refer to as the *return-flow solution*, is defined as follows:

$$\bar{u} = \tfrac{3}{4}z^2 - \tfrac{1}{2}z, \bar{v} = \bar{w} = 0, \bar{p} = \tfrac{3}{2}x, \qquad (2.7a,b,c,d)$$

$$\bar{T}_\infty = -x, \bar{Q} = 0. \qquad 2.7f,g)$$

The layer has a flat top, and the constant horizontal (axial) pressure gradient drives a return flow in the layer which maintains zero mass flux through any vertical plane. The x-component of velocity is parabolic in z (i.e. a sum of plane Couette and plane Poiseuille flows). The temperature field is linear in x as imposed, and the flow-induced temperature distribution makes the fluid at the lower plate cooler than that at the interface.

The return-flow solution arises from the consideration of the thermocapillary flow of a liquid contained in a two-dimensional slot, as shown in figure 3. This slot has depth d and length l, and its aspect ratio is defined as

$$A \equiv d/l. \qquad (2.8)$$

When a temperature gradient is imposed along the interface by fixing the temperatures of the ends of the slot, thermocapillary effects will drive a flow that can be approximated asymptotically as $A \to 0$. In this case, there can be at leading order a core region away from the ends composed of a parallel flow with zero mass flux through any vertical plane and end regions of dimension $O(A)$ where the fluid turns around. The solutions in these two regions are connected through asymptotic matching. The asymptotic solution for this problem was carried out in detail by Sen & Davis (1982).

In this asymptotic solution, surface curvature is needed to satisfy the contact-angle conditions at the ends. When $S \to \infty$, we are necessarily limited to a contact angle of 90°, which is the only one consistent with a non-deformable free surface. However, in the core region of the slot the boundary conditions at the slot ends are not considered in solving for the flow field, and so we can properly consider the limit of $S \to \infty$. In this limit, we find that the leading-order solution obtained by the asymptotic analysis of Sen & Davis (1982) becomes an exact solution of the outer problem, i.e. all $O(A)$ terms are identically zero.

In the subsequent stability analysis we shall consider the following generalized parallel-flow solution:

$$\bar{u} = \bar{u}'(1)\,z + \tfrac{1}{2}\bar{u}''(1)\,(z^2 - 2z), \tag{2.9a}$$

$$\bar{v} = \bar{w} = 0, \tag{2.9b, c}$$

$$\bar{p}_x = \bar{u}''(1), \tag{2.9d}$$

$$\bar{T} = -\bar{u}'(1)\,x + M\bar{u}'(1)\{\tfrac{1}{24}\bar{u}''(1)\,(1-z^4) + \tfrac{1}{6}[\bar{u}'(1) - \bar{u}''(1)]\,(1-z^3)\}, \tag{2.9e}$$

$$\bar{T}_\infty = -x, \tag{2.9f}$$

$$\bar{Q} = -\bar{T}_z|_{z=1}. \tag{2.9g}$$

When $\bar{u}'(1) = 1$ and $\bar{u}''(1) = 0$ we obtain the linear-flow solution. When $\bar{u}'(1) = 1$ and $\bar{u}''(1) = \frac{3}{2}$ we obtain the return-flow solution.

Note that in our linear stability analysis of the return-flow solution we shall allow M and R to be $O(1)$ with respect to A, while the complete analysis of Sen & Davis (1982) required that these be $O(A)$. As noted by Sen & Davis, this is *not* a contradiction, since the return-flow solution (2.7) remains a valid approximation to the core flow of the slot even when M and R are $O(1)$. This new ordering, however, will change the flow in the end regions, which we here ignore, and will change the $O(A)$ correction to the surface deflection, which vanishes in the limit of $S \to \infty$.

2.3. *The linearized disturbance equations*

In a standard way, we apply infinitesimal disturbances to the system defined by (2.3)–(2.5) as follows:

$$(\boldsymbol{v}, p, T) = (\bar{\boldsymbol{v}}, \bar{p}, \bar{T}) + (\boldsymbol{v}', p', T'). \tag{2.10}$$

After substitution into the governing equations and boundary conditions we linearize the system and obtain the following linear disturbance equations:

$$R\left[\frac{\partial v_i'}{\partial t} + \bar{u}\frac{\partial v_i'}{\partial x} + \frac{\mathrm{d}\bar{u}}{\mathrm{d}z}w'T_i\right] = -p'_{,i} + \nabla^2 v_i', \tag{2.11a}$$

$$M\left[\frac{\partial T'}{\partial t} + \bar{u}\frac{\partial T'}{\partial x} + \frac{\partial \bar{T}}{\partial x}u' + \frac{\partial \bar{T}}{\partial z}w'\right] = \nabla^2 T', \tag{2.11b}$$

$$v'_{i,i} = 0, \tag{2.11c}$$

$$v_i' = \frac{\partial T'}{\partial z} = 0 \quad \text{on} \quad z = 0, \tag{2.11d, e}$$

$$w' = 0 \quad \text{on} \quad z = 1, \tag{2.11f}$$

$$\frac{\partial u'}{\partial z} + \frac{\partial T'}{\partial x} = 0 \quad \text{on} \quad z = 1, \tag{2.11g}$$

$$\frac{\partial v'}{\partial z} + \frac{\partial T'}{\partial y} = 0 \quad \text{on} \quad z = 1, \tag{2.11h}$$

$$\frac{\partial T'}{\partial z} + BT' = 0 \quad \text{on} \quad z = 1, \tag{2.11i}$$

where

$$T_i = (1, 0, 0)_i. \tag{2.11j}$$

To solve this system we assume normal modes of the form

$$\{u', v', w', p', T'\} = \{\hat{u}(z), \hat{v}(z), \hat{w}(z), \hat{p}(z), \hat{T}(z)\} \exp[\mathrm{i}(\alpha x + \beta y - \sigma t)], \tag{2.12}$$

where α and β are disturbance wavenumbers in the x- and y-directions respectively.

In this form, the disturbance is assumed to be a wave travelling in a direction

$$\phi = \tan^{-1}\frac{\beta}{\alpha} \tag{2.13a}$$

with respect to the positive x-axis and with an overall wavenumber

$$k = (\alpha^2+\beta^2)^{\frac{1}{2}}. \tag{2.13b}$$

The complex eigenvalue

$$\sigma = \sigma_{\mathrm{R}} + \mathrm{i}\sigma_{\mathrm{I}} \tag{2.14}$$

contains the growth rate σ_{I} and the phase speed $c_{\mathrm{R}} = \sigma_{\mathrm{R}}/k$ of the disturbance.

The disturbance equations in normal-mode form are

$$\{\mathrm{D}^2-(\alpha^2+\beta^2)-\mathrm{i}\alpha R\bar{u}+\mathrm{i}R\sigma\}\,\hat{u} = \mathrm{i}\alpha\hat{p}+R\,\mathrm{D}\bar{u}\,\hat{w}, \tag{2.15a}$$

$$\{\mathrm{D}^2-(\alpha^2+\beta^2)-\mathrm{i}\alpha R\bar{u}+\mathrm{i}R\sigma\}\,\hat{v} = \mathrm{i}\beta\hat{p}, \tag{2.15b}$$

$$\{\mathrm{D}^2-(\alpha^2+\beta^2)-\mathrm{i}\alpha R\bar{u}+\mathrm{i}R\sigma\}\,\hat{w} = \mathrm{D}\hat{p}, \tag{2.15c}$$

$$\{\mathrm{D}^2-(\alpha^2+\beta^2)-\mathrm{i}\alpha M\bar{u}+\mathrm{i}M\sigma\}\,\hat{T} = M\bar{T}_x\,\hat{u}+M\bar{T}_z\,\hat{w}, \tag{2.15d}$$

$$\mathrm{D}\hat{w}+\mathrm{i}\alpha\hat{u}+\mathrm{i}\beta\hat{v} = 0, \tag{2.15e}$$

$$\hat{u} = \hat{v} = \hat{w} = \mathrm{D}\hat{T} = 0 \quad \text{on} \quad z = 0, \tag{2.15f}$$

$$\hat{w} = 0 \quad \text{on} \quad z = 1, \tag{2.15g}$$

$$\mathrm{D}\hat{u}+\mathrm{i}\alpha\hat{T} = 0 \quad \text{on} \quad z = 1, \tag{2.15h}$$

$$\mathrm{D}\hat{v}+\mathrm{i}\beta\hat{T} = 0 \quad \text{on} \quad z = 1, \tag{2.15i}$$

$$\mathrm{D}\hat{T}+B\hat{T} = 0 \quad \text{on} \quad z = 1, \tag{2.15j}$$

where $\mathrm{D} \equiv \mathrm{d}/\mathrm{d}z$ and alphabetic subscripts denote partial differentiation.

3. Method of solution: $\alpha \equiv 0$

System (2.15) must be solved numerically to characterize completely the three-dimensional instability of the basic state. However, we first restrict ourselves here to the special case of $\alpha \equiv 0$. This permits us to examine a simplified problem and thus to study the essential physics of the instability mechanism. The general disturbance will be treated in §5.

For $\alpha = 0$ the continuity equation can be used to eliminate $\hat{v}$ and $\hat{p}$, and we obtain the following system:

$$\{\mathrm{L}+\mathrm{i}\nu Pr^{-1}\}\,\hat{u} = MPr^{-1}\,\mathrm{D}\bar{u}\,\hat{w}, \tag{3.1a}$$

$$\{\mathrm{L}+\mathrm{i}\nu Pr^{-1}\}\,\mathrm{L}\hat{w} = 0, \tag{3.1b}$$

$$\{\mathrm{L}+\mathrm{i}\nu\}\,\hat{T} = M\bar{T}_x\,\hat{u}+M\bar{T}_z\,\hat{w}, \tag{3.1c}$$

$$\hat{u} = \hat{w} = \mathrm{D}\hat{w} = \mathrm{D}\hat{T} = 0 \quad \text{on} \quad z = 0, \tag{3.1d}$$

$$\mathrm{D}\hat{u} = \hat{w} = \mathrm{D}^2\hat{w}+\beta^2\hat{T} = \mathrm{D}\hat{T}+B\hat{T} = 0 \quad \text{on} \quad z = 1, \tag{3.1e}$$

where

$$\mathrm{L} \equiv \mathrm{D}^2-\beta^2, \tag{3.1f}$$

and

$$\nu \equiv M\sigma \tag{3.1g}$$

is the complex eigenvalue of this system. In this form ν is the complex frequency of the oscillations normalized with respect to the thermal-diffusion timescale.

System (3.1) can be solved exactly. Since we are interested in the neutral conditions of the instability, we set the growth rate of the disturbance to zero, and seek the real eigenvalue of the system

$$\nu_R = M\sigma_R. \tag{3.2}$$

If we normalize the eigenfunction as

$$\hat{T}(1) = 1, \tag{3.3}$$

then we can solve for $\hat{w}$ in (3.1*b*) and use $\hat{w}$ to find $\hat{u}$ from (3.1*a*). Knowing these two components of the velocity field, we can compute $\hat{T}$ from (3.1*c*). We find that $\hat{T}$ has the form

$$\hat{T} = M^2\theta[z;\, \nu_R,\, \beta,\, Pr,\, B,\, \bar{u}'(1),\, \bar{u}''(1)], \tag{3.4}$$

where $\theta = \theta_R + i\theta_I$ is a complex function. Using the normalization (3.3), we obtain the characteristic equation for the eigenvalue ν_R:

$$\theta_I[1;\, \nu_R,\, \beta,\, Pr,\, B,\, \bar{u}'(1),\, \bar{u}''(1)] = 0. \tag{3.5}$$

We use the secant method to determine numerically the root ν_R of this equation as a function of the other parameters. Then the value of M on the neutral curve is found from

$$M = \theta_R[1;\, \nu_R,\, \beta,\, Pr,\, B,\, \bar{u}'(1),\, \bar{u}''(1)]^{-\frac{1}{2}}, \tag{3.6}$$

and the associated σ_R is obtained from (3.2), i.e.

$$\sigma_R = \nu_R M^{-1}. \tag{3.7}$$

4. Results: $\alpha = 0$

4.1. *Linear flow: longitudinal rolls*

For the moment we follow Pearson (1958) and assume the stationary onset of instability by setting $\sigma_R = 0$. The resulting instability takes the form of stationary longitudinal rolls whose axes are aligned in the direction of the bulk flow. Neutral curves for $Pr = \infty$ and for several values of B are presented in figure 4. The minimum of these curves defines a critical Marangoni number M_c and a critical wavenumber β_c. The increasing behaviour of these critical parameters with B is readily apparent.

The neutral curve for $B = 0$ displays the most interesting behaviour. For $Pr = \infty$ it intersects the $\beta = 0$ line at $M = 15.49 = \sqrt{240}$, although its minimum occurs at $\beta = 0.52$. As Pr decreases, the value of M at the intersection increases, until at $Pr = 2$ the neutral curve asymptotes to the line $\beta = 0$. Decreasing Pr further moves the vertical asymptote to larger values of β. This behaviour of the neutral curves is shown in figure 5. The sensitivity of M_c to changes in Pr with $B = 0$ and $B = 1$ is shown in the right-hand curves of figure 6.

In figure 7(*a*) we show the projection of neutral-disturbance streamlines on a cross-section of the layer at a constant x-location for $Pr = 2.0$. For large Pr the rolls are very wide with respect to the depth of the layer. The width of the rolls depends inversely on the critical wavenumber β_c and decreases with decreasing Pr. The dependence of the critical wavenumber β_c versus the Prandtl number for $B = 0$ is shown in curve (*d*) of figure 15. The centre of each roll is located near the surface, in keeping with an instability driven by surface forces.

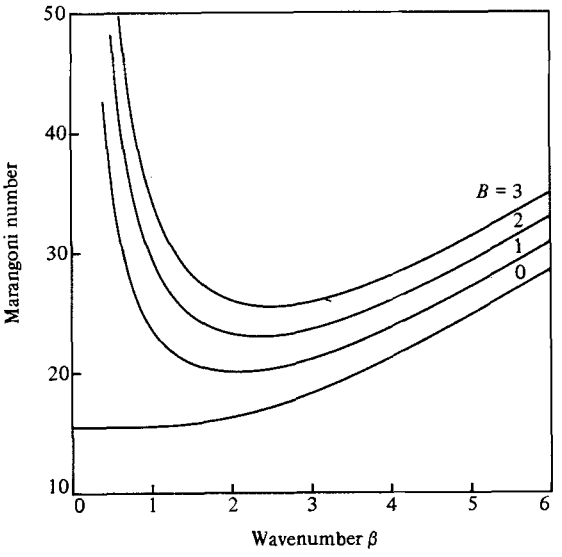

FIGURE 4. Neutral curves for longitudinal rolls in the linear flow with $Pr = \infty$ and various values of B.

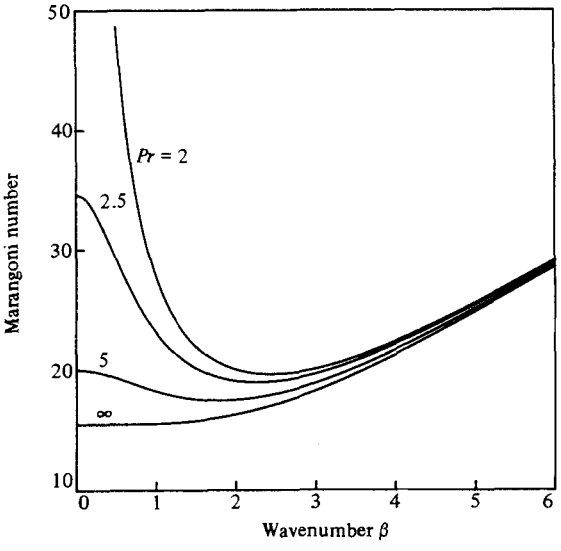

FIGURE 5. Neutral curves for longitudinal rolls in the linear flow with $B = 0$ and various values of Pr.

4.2. *Linear flow: hydrothermal waves*

For non-zero values of σ_R the characteristic equation (3.5) must be solved numerically to obtain the eigenvalue ν_R. In this case the instability is in the form of longitudinal hydrothermal waves that propagate in *either normal direction* to the basic flow. Neutral curves for $Pr = 0.5$ and several values of B are presented in figure 8. As with longitudinal rolls, increasing the heat transfer from the surface of the layer leads to a more stable system.

Also shown in figure 8 are the neutral curves for longitudinal rolls when $Pr = 0.5$. Here we see that for each value of B the neutral curve for hydrothermal waves

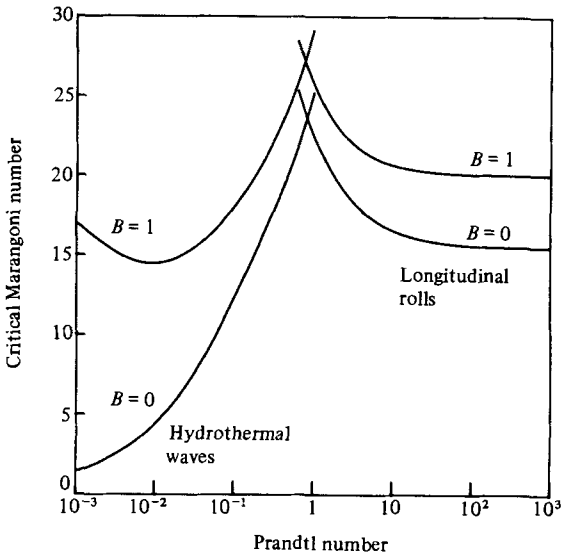

FIGURE 6. The critical Marangoni number versus Pr for both longitudinal rolls and hydrothermal waves in the linear flow with $B = 0$ and $B = 1$.

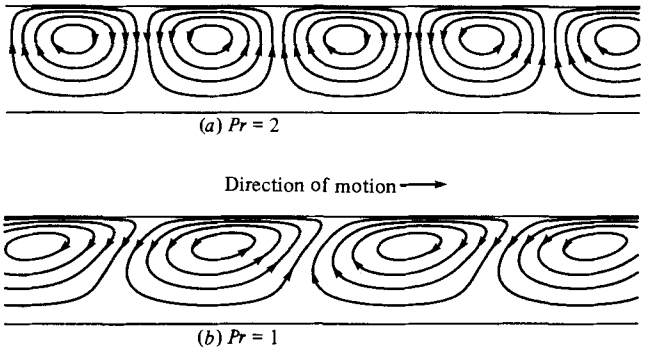

FIGURE 7. The projected streamlines at a constant x-location. (*a*) is for stationary longitudinal rolls in the linear flow, and (*b*) is for longitudinal hydrothermal waves in the return flow.

branches off the neutral curve for longitudinal rolls. At the branch point the frequency $\nu_R = 0$, and it increases as one moves to the left along the hydrothermal-wave curve.

In figure 9 we set $B = 0$ and examine the dependence of the neutral curves on Pr. For small Pr, the hydrothermal-wave neutral curve branches off from the neutral curve for longitudinal rolls at a point to the right of the minimum. As Pr increases, this branch point moves to the left past the minimum and up the neutral curve until it reaches infinity when $Pr = 2$. For larger values of Pr, hydrothermal waves do not exist. The sensitivity of M_c to changes in Pr with $B = 0$ and $B = 1$ is also shown in figure 6. In figure 6 we see that the crossover point for the two modes when $B = 0$ is $Pr = 0.82$. For $Pr > 0.82$, the layer is unstable to longitudinal rolls, while, for $Pr < 0.82$, the layer is unstable to hydrothermal waves. When $B = 1$ the crossover point is $Pr = 0.77$.

The projection of some neutral-disturbance streamlines on a cross-section of the layer at a constant x-location would be similar to those shown in figure 7 (*b*). These

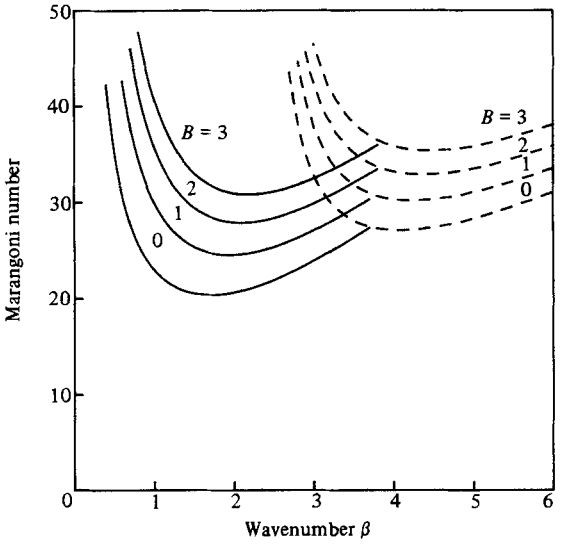

FIGURE 8. Neutral curves for longitudinal rolls and hydrothermal waves in the linear flow with $Pr = 0.5$ and various values of B. The longitudinal-roll neutral curves are the dashed lines.

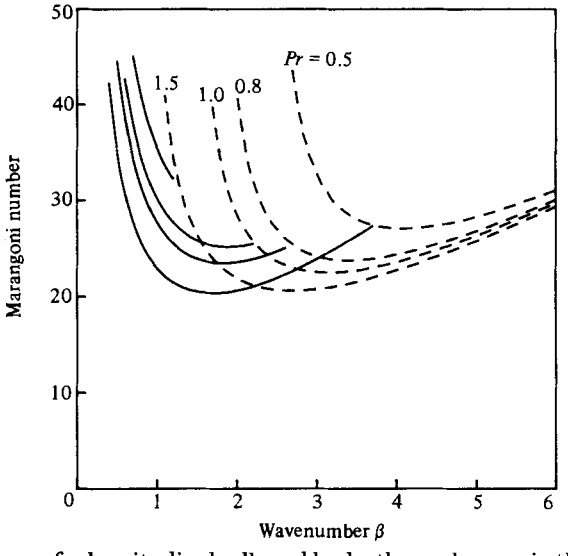

FIGURE 9. Neutral curves for longitudinal rolls and hydrothermal waves in the linear flow with $B = 0$ and various values of Pr. The longitudinal-roll neutral curves are the dashed lines.

streamlines also exhibit a roll-like structure, but they have an asymmetric deformity compared with the stationary rolls shown in figure 7 (*a*). The deformation occurs as a slanting of the rolls in the direction of their propagation, which is to the right in the case shown.

4.3. *Return flow: stationary rolls*

There are no stationary-roll instabilities for the return flow. The reason is apparent when one considers the mechanism of the instability. We shall discuss this in §7.

4.4. *Return flow: hydrothermal waves*

The hydrothermal wave instability is documented for the return flow in figures 10–12. Note that the return flow is much more stable (i.e. has higher critical Marangoni

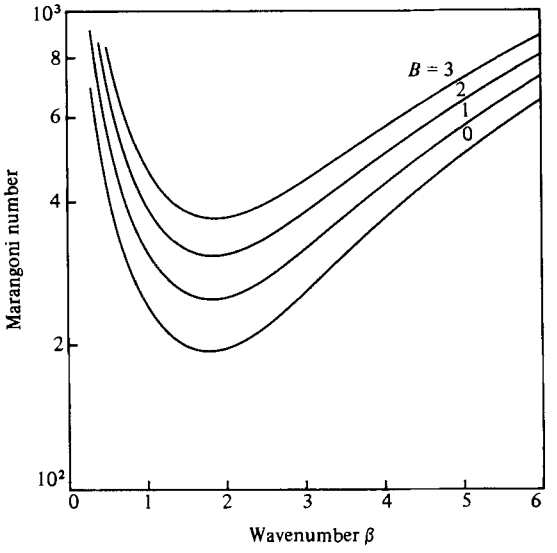

FIGURE 10. Neutral curves for hydrothermal waves in the return flow with $Pr = 1.0$ and various values of B.

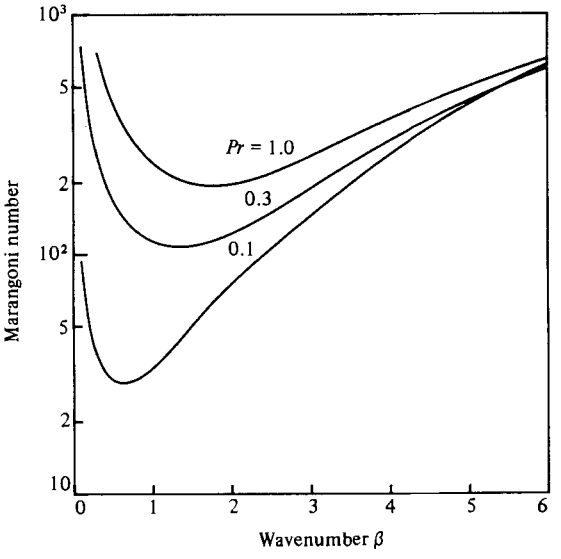

FIGURE 11. Neutral curves for hydrothermal waves in the return flow with $B = 0$ and various values of Pr.

numbers) than the linear flow, while its critical wavenumbers are only slightly smaller. The projection of the disturbance streamlines on a cross-section of the layer at a constant x-location is shown explicitly in figure 7 (b) for $Pr = 1$.

5. Method of minimization: $\alpha \neq 0$

In §3 our selection of a longitudinally oriented disturbance, i.e. $\alpha \equiv 0$, led to an exact solution of the linearized disturbance equations from which two types of thermal instabilities were found: steady longitudinal rolls and longitudinal travelling hydrothermal waves. However, we have no assurance that $\alpha = 0$ corresponds to the most

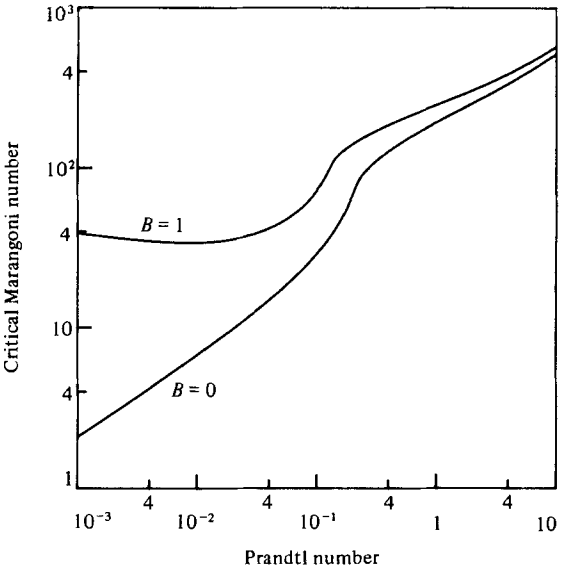

FIGURE 12. The critical Marangoni number versus Pr for hydrothermal waves in the return flow with $B = 0$ and $B = 1$.

dangerous mode for either of these instabilities, because a Squire's theorem for this flow is not possible.† Thus, we must solve the complete three-dimensional disturbance equations (2.15) and minimize the neutral value of the Marangoni number over (α, β)-parameter space to find the most dangerous (α, β)-pair. From the results of the minimization, we shall be able to describe the preferred mode of instability in the entire range of Pr for each of the basic-state flow fields being considered.

The three-dimensional disturbance equations (2.15) are solved numerically using the computer code called SUPORT written by Scott & Watts (1975, 1977). From this calculation and subsequent uses of the secant method we obtain the Marangoni number at the point of neutral stability M_N and thus define a neutral surface in the form

$$M_N = M_N[\alpha, \beta; Pr, B, \bar{u}'(1), \bar{u}''(1)]. \tag{5.1}$$

The critical Marangoni number M_c is defined as the global minimum of the neutral surface. The location of this minimum (α_c, β_c) is found as follows.

We make an initial guess for (α_c, β_c), estimate the local tangent plane to the neutral surface at this point and then increment (α, β) by a small amount in the direction of steepest descent. We iterate in this manner until a local minimum of the neutral surface M_m is found at the point (α_m, β_m). This sequence of iterations is repeated for several values of the Prandtl number in the range $(0, \infty)$. From the resulting curves of M_m versus Pr we identify the critical Marangoni number of the system as the smallest value of M_m for each Pr. The corresponding values of $(\alpha_m, \beta_m) = (\alpha_c, \beta_c)$ and so define the (x, y)-structure of the preferred mode of instability.

† Gumerman & Homsy (1974) investigated the interaction of a surface-tension-driven convective instability with an imposed shear flow by considering a concurrent two-phase Couette flow with an independently applied vertical temperature gradient. In their work, as well as in others involving stratified shear flows, a Squire's transformation is shown to exist though it does not lead to a Squire's theorem. However, in the present problem the imposed horizontal temperature gradient produces the shear flow. Because of this tight coupling, even a Squire's transformation *does not* exist.

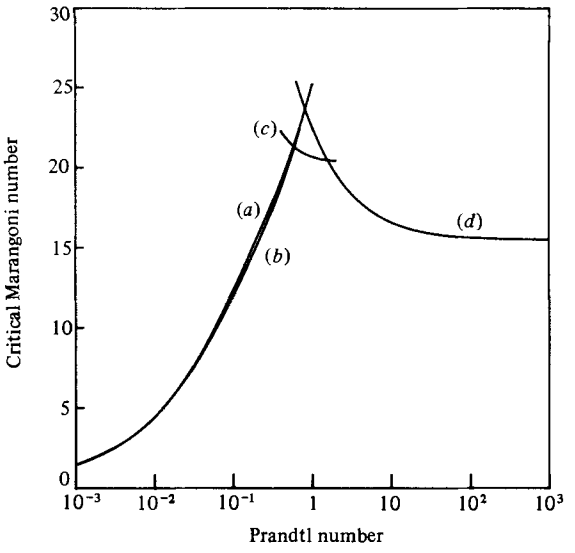

FIGURE 13. The critical Marangoni number M_c versus the Prandtl number for the linear flow with $B = 0$. Curve (*a*) is for longitudinal hydrothermal waves, (*b*) is for oblique hydrothermal waves, (*c*) is for two-dimensional hydrothermal waves and (*d*) is for longitudinal rolls. The lowest value of M for each Pr defines M_c for the preferred mode.

6. Results: $\alpha \neq 0$

In §4 we saw that an increase in the Biot number B always results in a more stable system. This behaviour also occurs when $\alpha \neq 0$. Thus, to simply the following discussion we shall confine ourselves to the case $B = 0$ and then minimize the Marangoni number over the neutral surface as described earlier to obtain the preferred mode of instability as a function of Pr only.

6.1. *Linear flow*

For $Pr < 0.60$ the preferred mode consists of two hydrothermal waves propagating at the angles $\pm\psi$ with respect to the *negative* x-axis, where

$$\psi = |\phi| \tag{6.1}$$

and ϕ is defined in (2.13*a*). The M_c versus Pr curve for these waves is shown in figure 13 along with the corresponding curve for longitudinal hydrothermal waves. The maximum decrease in M_c for the oblique waves with respect to the longitudinal waves is 3.2%, occurring at $Pr = 0.2$. As $Pr \to 0$, the two curves become indistinguishable. Our numerical calculations show that for both curves $M_c \sim Pr^{\frac{1}{2}}$ as $Pr \to 0$. Thus the preferred mode of hydrothermal waves is 'nearly' the longitudinal wave.

In figure 14 we show how the angle of propagation ψ varies with Pr. As $Pr \to 0$, $\psi \to 90°$. Thus the preferred mode for small Pr is the longitudinal wave. The smallest angle of propagation is 82.5°, occurring at about $Pr = 0.4$. From the known error of ± 0.01 for both wavenumbers α and β we can compute the error $\delta\psi$ for the angle ψ. When $Pr > 0.1$, $|\delta\psi| \leqslant 1.0°$. But, for $Pr = 0.01$, $|\delta\psi| = 2.2°$, and, for $Pr = 0.001$, $|\delta\psi| = 7.1°$. This decrease in accuracy is due to the decreasing magnitude of both α and β as $Pr \to 0$. Thus, while figure 14 shows the general trend for ψ when Pr is small, more accurate calculations are needed to define ψ precisely in this range.

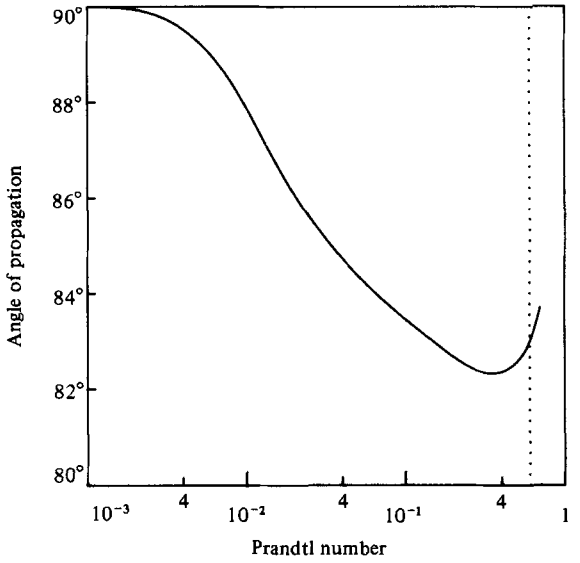

FIGURE 14. The angle of propagation ψ versus Prandtl number for the preferred mode of oblique hydrothermal waves in the linear flow with $B = 0$. The error $|\delta\psi|$ is 7.1° at $Pr = 0.001$, 2.2° at $Pr = 0.01$ and $< 1°$ for $Pr > 0.1$.

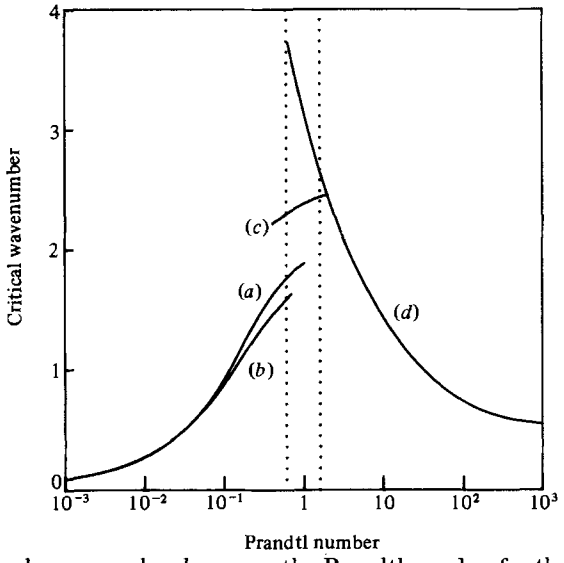

FIGURE 15. The critical wavenumber k_c versus the Prandtl number for the linear flow with $B = 0$. Curve (*a*) is for longitudinal hydrothermal waves, (*b*) is for oblique hydrothermal waves, (*c*) is for two-dimensional hydrothermal waves and (*d*) is for longitudinal rolls. The dotted vertical lines are at $Pr = 0.60$ and $Pr = 1.60$. Curves (*b*)–(*d*) are for the preferred mode.

In figures 15 and 16 we show the critical wavenumber and the critical phase speed versus Pr for the preferred mode. The critical frequency is defined as

$$f_c = \frac{k_c c_{Rc}}{2\pi}. \tag{6.2}$$

When $0.60 < Pr < 1.60$, the preferred mode is a two-dimensional hydrothermal wave, i.e. $\beta \equiv 0$, propagating in the direction of the surface flow. The curves of M_c, α_c and c_{Rc} versus Pr for this mode are also shown in figures 13, 15 and 16 respectively.

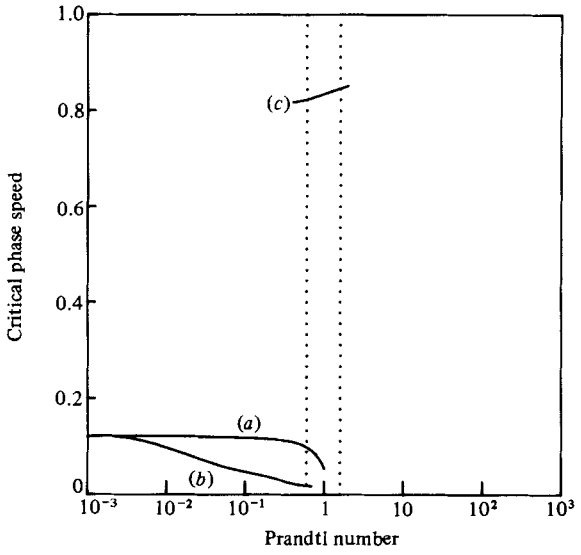

FIGURE 16. The critical phase speed c_{Rc} versus the Prandtl number for the linear flow with $B = 0$. Curve (*a*) is for longitudinal hydrothermal waves, (*b*) is for oblique hydrothermal waves and (*c*) is for two-dimensional hydrothermal waves. The dotted vertical lines are at $Pr = 0.60$ and $Pr = 1.60$. Curves (*b*) and (*c*) are for the preferred mode. For $Pr > 1.60$ the preferred phase speed is zero.

For all values of $Pr > 1.6$ longitudinal rolls are preferred. In addition, our numerical calculations have also shown that $\alpha = 0$ is the only possible stationary mode. For comparison, the curves of M_c and β_c versus Pr for this mode are shown in figures 13 and 15 respectively.

6.2. *Return flow*

For all values of Pr, the preferred mode of instability is a hydrothermal wave propagating at the angles $\pm\psi$ with respect to the *negative* x-axis. In figure 17 we present M_c versus Pr for this preferred mode, for the longitudinal waves of §§3 and 4, i.e. with $\alpha \equiv 0$, and for the special case of two-dimensional waves, i.e. with $\beta \equiv 0$. As $Pr \to 0$, M_c for the preferred mode approaches the value of M_c for longitudinal waves. At $Pr = 0.001$ the difference between these two values is $-5.5\,\%$. As in the linear-flow case, $M_c \sim Pr^{\frac{1}{2}}$ as $Pr \to 0$. When $Pr \to \infty$, $M_c \to 398.5$ for the preferred mode. This is a decrease of $0.02\,\%$ from the limiting value of M_c for two-dimensional waves.

The angle of propagation ψ versus Pr is shown in figure 18. As Pr gets small, ψ starts to approach 90°. However, the accuracy problem for ψ discussed earlier also exists here. For $Pr > 0.1$, $|\delta\psi| < 1.1°$, but, at $Pr = 0.01$, $|\delta\psi| = 2.9°$, and, for $Pr = 0.001$, $|\delta\psi| = 8.4°$. Thus the maximum that occurs in figure 18 for small Pr may be due to the large errors involved in calculating ψ. As Pr increases, ψ decreases smoothly and approaches a limiting value of $7.9° \pm 0.26°$ as $Pr \to \infty$. In figures 19 and 20 we present the critical wavenumber and the critical phase speed versus Pr for the preferred mode. The limiting values as $Pr \to \infty$ are $k_c \to 2.47$ and $c_{Rc} \to 0.06220$.

7. Discussion

In order to characterize the mechanisms of instability we must first identify those terms in the governing equations that determine the eigenvalue of the problem. In

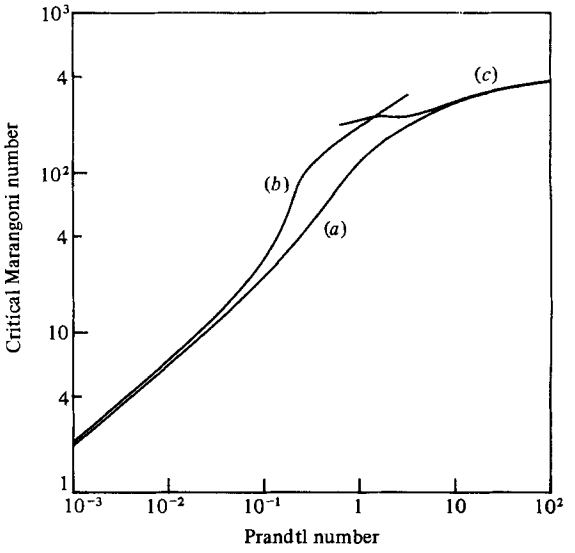

FIGURE 17. The critical Marangoni number M_c versus the Prandtl number for the return flow with $B = 0$. Curve (a) is for the preferred mode of oblique hydrothermal waves, (b) is for longitudinal hydrothermal waves and (c) is for two-dimensional hydrothermal waves.

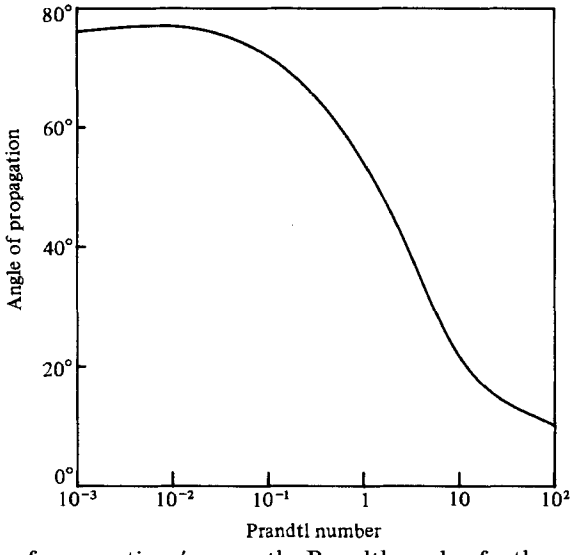

FIGURE 18. The angle of propagation ψ versus the Prandtl number for the preferred mode of oblique hydrothermal waves in the return flow with $B = 0$. The error $|\delta\psi|$ is 8.4° at $Pr = 0.001$, 2.9° at $Pr = 0.01$ and smaller than 1° for $Pr > 0.1$.

(2.15), which governs the three-dimensional instability of the layers, the velocity field is coupled to the temperature field through the thermocapillary shear-stress conditions on the interface, viz (2.15h,i). Because of this simple coupling, we can find the corresponding velocity field in the layer for any arbitrary temperature disturbance of the free surface. In effect, the coupling acts as a simple forcing function for the velocity. Once the velocity field is known the eigenvalue of the system is found by solving the energy equation (2.15d). Thus the mechanism for the instability is associated with a balance between heat convection and heat conduction in the layer. The velocity field is important only as it transports heat in the system. Any

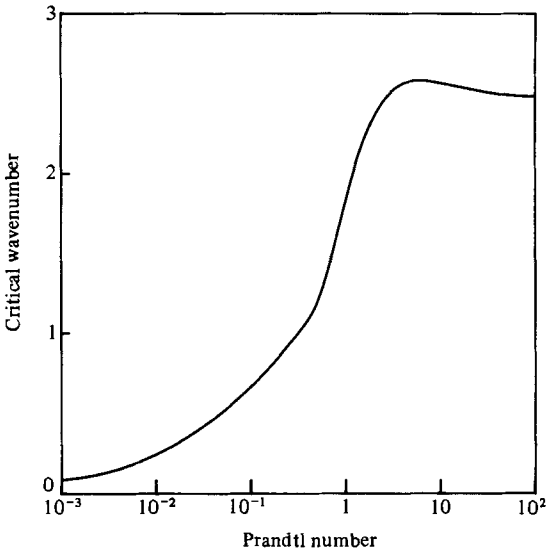

FIGURE 19. The critical wavenumber k_c versus the Prandtl number for the preferred mode of oblique hydrothermal waves in the return flow with $B = 0$.

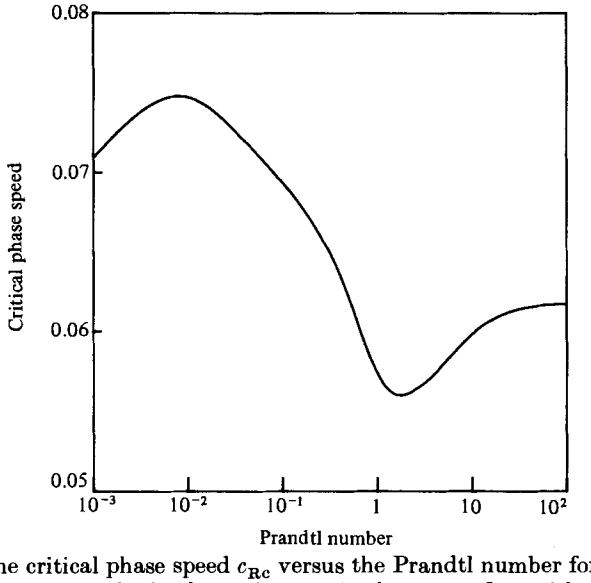

FIGURE 20. The critical phase speed c_{Rc} versus the Prandtl number for the preferred mode of oblique hydrothermal waves in the return flow with $B = 0$.

mechanical aspects of the velocity field, such as viscous dissipation, are not important in terms of the fundamental mechanisms of the instabilities.

7.1. *Longitudinal rolls*

In a static liquid layer heated from below, classical Marangoni convection cells appear when the temperature gradient normal to the layer is sufficiently large, as shown by Pearson (1958). The mechanism for this instability is described as follows. Consider a local hot spot on the interface of the layer due to some random temperature perturbation. Thermocapillarity will produce a surface flow that draws fluid away from this point. By continuity, a vertical velocity field is established that convects

hotter fluid from the interior of the layer to the hot spot on the interface. If the temperature gradient across the layer is sufficiently large, the transport of heat by convection will be enough to balance or exceed the losses due to heat conduction away from the interface. Thus, the elevated temperature of the hot spot will be maintained or increased and the convection will continue.

The basic-state temperature field for the linear flow given by (2.6*c*) contains a flow-induced vertical distribution corresponding to the layer being 'heated from below'. Thus there is the possibility that a stationary convective instability, as described by Pearson (1958), can arise in this case. We find that such a situation can arise only if $\alpha = 0$, i.e. if the disturbances form longitudinal rolls. In a static liquid layer there is a symmetry attained for every (α, β)-pair, and so the planform of the classical Marangoni convection cell cannot be determined from linear theory. The addition of a basic-state velocity field eliminates this degeneracy in favour of a stationary longitudinal disturbance.† From the results of the three-dimensional minimization, we have found that longitudinal rolls are the preferred mode for $B = 0$ for $Pr > 1.6$ and that $\alpha = 0$ is the only possible stationary mode.

As the Prandtl number of the fluid is decreased, the critical Marangoni number and the critical wavenumber of the instability increase. This behaviour has been explained through the use of an energetics analysis which shows how the energy from the basic flow is transferred to the disturbances. Details of this analysis can be found in Smith (1982). The results of the analysis show that the increasing behaviour of M_c and β_c with decreasing Pr is due to the stabilizing effect of heat convection by horizontal velocity perturbations. The horizontal velocity field u' occurs as a result of the coupling between the vertical disturbance velocity and the horizontal basic-state velocity field in the convective acceleration term of the momentum equation (3.1*a*). The magnitude of u' is proportional to Pr^{-1}. When $Pr \to \infty$ for a fixed Marangoni number, viscous forces dominate in setting up the velocity field in the layer and $u' = 0$. For finite values of Pr, the convective acceleration term in the momentum equation causes $u' < 0$ when underneath a hot spot on the interface. This in turn produces a convective cooling of the interface which tends to stabilize the layer. Thus, for a fixed M and β, as the Prandtl number of the fluid is decreased, the layer will become more stable.

To move the system back to the critical neutral point for this decreased value of Pr, the convective heating of the hot spot on the interface must be increased. This can be done by increasing the Marangoni number, which increases the vertical temperature gradients and the magnitude of u' at the same rate, or by increasing the wavenumber, i.e. decreasing the width of the roll, which increases the magnitude of the horizontal and the vertical disturbance velocities in the layer. Increasing the wavenumber of the roll also increases the thermal dissipation in the layer, but at a slower rate than the increase in the convective heating. Thus a new critical neutral point is established at a higher Marangoni number and a larger wavenumber. It is important to note that the decrease in the width of the roll as Pr decreases lies in the effect of Pr on the convective heating of the interface as shown above and not in the use of Pr as a measure of the viscous dissipation in the layer.

† Similarly, Gumerman & Homsy (1974) also find that the presence of a shear flow eliminates the degeneracy of the static layer. In their work, however, the longitudinal roll does not interact with the underlying shear flow, and so the stability characteristics are the same as those of the classical static layer. In the present problem, the roll *does* interact with the shear flow through the horizontal temperature field and so has stability characteristics different from the static layer.

The physical mechanism for the instability as discussed earlier can now be modified to include the effects of the non-static basic-state velocity field for finite values of the Prandtl number. A hot fluid line on the interface of the layer parallel to the x-axis produces a vertical velocity field just as before that convects the warmer fluid from the interior of the layer to the interface. As each particle of fluid rises toward the hot line, it moves into a region where the basic-state velocity is higher than where it came from. This produces a negative horizontal velocity perturbation under the line that reduces the convective heating of the interface that occurs as a result of the horizontal basic-state temperature and velocity fields. If the temperature gradient in the x-direction is large enough, the net convective heating of the interface by these horizontal and vertical velocity perturbations will be enough to balance or exceed the losses due to thermal conduction away from the interface. Thus the elevated temperature of the hot line will be maintained or increased and the perturbation convection field will continue.

The return flow in the layer does not exhibit a stationary convective instability. The basic-state temperature field for the return flow given by (2.7*e*) contains a flow-induced vertical temperature distribution corresponding to the layer being 'cooled from below'. If a temperature disturbance in the form of a hot line develops on the interface, the resulting vertical velocity field will convect cooler fluid from the interior of the layer to the surface. Thus the convection field will tend to eliminate the disturbance and so unstable longitudinal rolls cannot form.

7.2. *Hydrothermal waves: linear flow*

For small values of the Prandtl number, a new unsteady mode of instability appears in the form of two mirror-image hydrothermal waves that propagate in an oblique direction with a component *opposite* to the direction of the surface flow.

For small Pr, the preferred mode is a purely longitudinal hydrothermal wave. As Pr increases, the angle of propagation ψ decreases from 90° to values about 83° as shown in figure 14. The results of the energetics analysis of Smith (1982) show that the mechanism of instability involves a transfer of energy from the (axial) horizontal basic-state temperature field to the disturbances through perturbations in the horizontal convection field. Physically, this mechanism can be described as follows. Consider a local temperature disturbance of the interface in the form of a hot line parallel to the x-axis oscillating at some characteristic frequency. Thermocapillarity and conservation of mass will produce an oscillating vertical velocity field with a phase lag less than 90° behind the oscillating temperature of the disturbance. Because of this favourable phase relationship the vertical velocity will generally be convecting warm fluid from the interior of the layer to the interface when the disturbance temperature is positive, and convecting fluid away from the interface to the warmer interior when the disturbance temperature is negative. The net result is an overall input of energy to the disturbance from vertical convection.

Since the viscous forces in the layer are small, a horizontal velocity perturbation will be induced as a result of the convective acceleration effects of the fluid moving vertically in a linear basic-state velocity field. This velocity perturbation will be phased less than 90° ahead of the temperature of the disturbance and so will generally increase the convective heating of the interface when the disturbance temperature is positive and reduce the convective heating when the disturbance is negative. The net result is a large input of energy to the disturbances from the horizontal convection.

For convenience, we define the effective heating of the interface as the total

convective heating minus the losses due to conduction. Now, if the temperature gradient along the layer is large enough, the effective heating of the interface by the disturbance will exactly balance the time rate of change of the interfacial disturbance temperature, and the effective heating will be phased exactly 90° ahead of this temperature. Thus the disturbance will be maintained. If the temperature gradient along the interface is even larger, the phasing will be less than 90° and the temperature disturbance will increase.

The mechanism of instability described above is critically dependent on the influence of convective acceleration effects in producing the horizontal velocity field. As the Prandtl number increases, these effects are decreased resulting in a decrease in the energy input to the disturbances from horizontal convection. Since the effective heating of the disturbance can be increased by increasing the Marangoni number and by decreasing the wavelength a new critical neutral point is established at larger values of M and k.

For $0.60 < Pr < 1.6$, two-dimensional hydrothermal waves become the preferred mode. Here, vertical convection is destabilizing. Holding M fixed, an increase in Pr will cause an increase in vertical convection and the layer becomes unstable. As a result, M_c decreases as Pr increases.

The largest value of $M_c = 21.27$ occurs at $Pr = 0.6$. Therefore, for $B = 0$ the linear flow is always unstable when $M > 21.27$.

7.3. *Return flow*

Since longitudinal rolls do not exist for the return flow in the layer, the preferred mode is always an obliquely travelling hydrothermal wave. As in the linear-flow case, the instability is close to being a longitudinal wave when Pr is small, and the layer becomes more stable as Pr increases because of the reduced convective heating of the interface.

The results of the energetics analysis (Smith 1982) show that for small Pr the mechanism of instability is a *transfer of energy from the horizontal basic-state temperature field to the disturbances through horizontal convection*. This is the same mechanism as for the small-Prandtl-number case in the linear flow. The basic difference between the two cases is that the flow-induced temperature distribution of the basic state is stabilizing for the return flow. For large values of Pr energy transfer from the vertical flow-induced temperature distribution to the disturbances through vertical convection becomes the dominant mechanism of instability.

When Pr is large, the thermal field exhibits large changes with depth. Thus a small increase in Pr produces large changes in the thermal field which result in increased thermal dissipation that stabilizes the layer. Larger Marangoni numbers are needed to increase the convective heating of the interface needed to produce neutral stability.

At $Pr = \infty$ the direction of propagation of the disturbances is only 7.90°. Thus a two-dimensional wave is a good approximation to the preferred mode for large Pr. Because $\psi < 90°$ for all Pr, the disturbance always propagates in a direction with a component in the direction opposite to that of the surface flow.

The largest value of $M_c = 398.5$ occurs at $Pr = \infty$. Therefore, for $B = 0$ the return flow is always unstable when $M > 395.8$.

7.4. *Application*

In tables 1 and 2 we present the results of an application of the theory to two specific liquid layers each 1 mm in depth and each having $B = 0$. We compute the following dimensional quantities: the critical wavelength λ_c, the critical frequency f_c^*, the

Parameter	Linear flow	Return flow
μ (g cm^{-1} s^{-1})	0.88×10^{-2}	—
k (erg s^{-1} cm^{-1} °C^{-1})	0.32×10^{7}	—
ρ (g cm^{-3})	2.5	—
c_p (erg g^{-1} °C^{-1})	0.84×10^{7}	—
σ (dyn cm^{-1})	720	—
γ (dyn cm^{-1} °C^{-1})	0.43	—
S	2.32×10^{6}	—
Pr	0.023	—
M_c	6.3	9.6
k_c	0.41	0.36
c_{Rc}	0.081	0.073
ψ	86	76
λ_c (cm)	1.5	1.75
f_c^* (Hz)	0.51	0.61
U_c (cm s^{-1})	9.6	14.7
c_{Rc}^* (cm s^{-1})	0.78	1.1
b_c (°C cm^{-1})	2.0	3.0
Ca	1.2×10^{-4}	1.8×10^{-4}

TABLE 1. An application of the theory to a 1 mm layer of liquid silicon at 1410 °C

Parameter	Linear flow	Return flow
μ (g cm^{-1} s^{-1})	2.78×10^{-2}	—
k (erg s^{-1} cm^{-1} °C^{-1})	5.65×10^{4}	—
ρ (g cm^{-3})	1.904	—
c_p (erg g^{-1} °C^{-1})	1.88×10^{7}	—
σ (dyn cm^{-1})	119	—
γ (dyn cm^{-1} °C^{-1})	0.07	—
S	2.93×10^{4}	—
Pr	9.25	—
M_c	16.7	267
k_c	1.48	2.56
c_{Rc}	0	0.060
ψ	90	23
λ_c (cm)	0.43	0.25
f_c^* (Hz)	0	1.0
U_c (cm s^{-1})	0.26	4.2
c_{Rc}^* (cm s^{-1})	0	0.25
b_c (°C cm^{-1})	1.0	17
Ca	6.2×10^{-5}	9.9×10^{-4}

TABLE 2. An application of the theory to a 1 mm layer of liquid $NaNO_3$ at 320 °C

critical surface speed U_c, the critical phase speed c_{Rc}^* and the critical temperature gradient b_c. The first layer, composed of liquid silicon, has a similar instability for both the linear and the return flow. This is due to its small $Pr = 0.023$. The instability takes the form of a hydrothermal wave propagating at $\pm 86°$ from the negative x-axis for the linear flow and $\pm 76°$ for the return flow. The frequency of the oscillations are 0.51 Hz and 0.61 Hz respectively, while the wavelengths are 15.0 and 17.5 times the depth respectively.

The second layer is composed of liquid $NaNO_3$, which has a $Pr = 9.25$. For the linear flow, the instability takes the form of longitudinal rolls a pair of which is about 4.3

times the depth of the layer. With the return flow, the instability is a hydrothermal wave propagating at $\pm 23°$ from the negative x-axis. Its frequency is 1 Hz and its wavelength is 2.5 times the layer depth.

The phase speed for the resulting hydrothermal waves is quite small in both examples, being about 6–8% of the free-surface speed. The free-surface speed is much smaller for the $NaNO_3$ layer than for the silicon layer because of the larger viscosity and the lower sensitivity of surface tension to temperature for $NaNO_3$.

The limit $S \to \infty$ results in an undeformed interface of the layer. The parameter that measures the magnitude of the surface deformation is the capillary number, defined as

$$Ca \equiv \frac{M}{Pr\,S}. \tag{7.1}$$

In each of the above examples, the capillary number for a neutral disturbance is about 10^{-3}–10^{-4}. Thus our assumption of a non-deformable free surface in the theory is reasonable.

Most of the experimental data available are those of Schwabe & Scharmann (1979) and Chun & Wuest (1979). These studies were done using a cylindrical half-floating-zone geometry. Thus comparison with our infinite-layer model can only be done in a qualitative sense. Our prediction of an obliquely travelling hydrothermal wave roughly corresponds to the instability seen in these experiments. For both studies the critical Marangoni number is about 10^4, where M has a lengthscale given by the axial length of the cylinder. Moreover, the aspect ratios are all near unity, so that the Marangoni numbers based on the scales used in this paper, where we equate the radius of the cylinder with depth, are still about 10^4. For $NaNO_3$ our computed M_c is about 267. This large difference in M_c between theory and experiment can be attributed to, among other things, the effects of a cylindrical geometry and to the end effects of a finite geometry. In addition, the thermal conditions we use on our layers are idealized, e.g. $\bar{T}_\infty$ is not necessarily linear in practice.

Because the phase speed of the disturbances does not change much over the entire range of Pr and thus with changes in M_c of two orders of magnitude, this might be in reasonable agreement with experiment. Chun & Wuest (1979) report that the phase speed of the disturbance in the azimuthal direction is on the order of 1% of the free-surface velocity for methanol. The Prandtl number of this fluid is 6.8, and we compute $c_{Rc} = 0.059$ and $\psi = 27°$. In the direction normal to the basic-state flow, the phase speed would be 0.03, which is qualitatively in agreement with the observed instability.

Chun & Wuest (1979) also discuss the mechanism of the thermocapillary instability that they observed experimentally. However, their mechanism ultimately rests on the results of a disturbance energy analysis for buoyancy-driven convection and so cannot apply. Smith (1982) did the disturbance energy analysis on the thermocapillary problem discussed in the present work. From these results, we were able to describe correct mechanisms for the thermocapillary instability.

8. Conclusions

The basic mechanism (Pearson 1958) that produces classical Marangoni convection cells can also operate in a thermocapillary shear layer to produce stationary longitudinal rolls. This will occur if the flow-induced basic-state temperature field corresponds to the layer being 'heated from below'. Viscous forces are primarily responsible for the steady convection field of this instability but, due to the non-zero

basic-state velocity, convective acceleration effects induce a stabilizing horizontal velocity perturbation that increases as Pr decreases. As a result, the critical Marangoni number and the critical wavenumber depend on the Prandtl number.

We also find a *new oscillatory instability* that takes the form of two hydrothermal waves that propagate obliquely to the direction of the surface flow. The mechanism for this instability involves the transfer of energy from the horizontal (axial) basic-state temperature field to the disturbances through horizontal convection when Pr is small, and the transfer of energy from the vertical basic-state temperature field to the disturbances through vertical convection when Pr is large. Convective acceleration effects become very important in setting up the oscillating convection field for this mode.

For a linear flow with $B = 0$, oblique hydrothermal waves are the preferred mode of instability when $Pr < 0.6$, and two-dimensional hydrothermal waves are preferred when $0.6 < Pr < 1.6$. If $Pr > 1.6$, longitudinal rolls are preferred.

For a return flow, hydrothermal waves exist over the entire range of the Prandtl number. The critical Marangoni number is always slightly larger than the M_c for a linear flow and the critical wavenumber always slightly less for small values of Pr. For large Pr, M_c is an order of magnitude greater than M_c for longitudinal rolls.

The linear-theory problem for a static liquid layer is degenerate in that the planform of the instability cannot be determined (Scanlon & Segel 1967). The form of the disturbance, i.e. hexagonal cells, is selected by nonlinear effects. In the dynamic layer, a degeneracy occurs for hydrothermal waves in that two sets of waves become unstable at the same time, one moving with a component in the positive y-direction and one in the negative y-direction. Thus the preferred form of the disturbance, i.e. an oblique right-moving wave, an oblique left-moving wave or some combination of the two, can also be selected by nonlinear interaction.

Both Schwabe & Scharmann (1979) and Chun & Wuest (1979) have documented the existence of an oscillatory instability in the thermocapillary convection field of a cylindrical floating zone. The return-flow solution would be the two-dimensional analogue of the cylindrical velocity field. The qualitative agreement between our theory and these experiments gives us encouragement that the mechanism which causes hydrothermal waves in an infinite layer will produce the same instability in a cylindrical geometry.

This research was supported through contract no. NAS8-33881, National Aeronautics and Space Administration; Material-Processing-in-Space Program.

REFERENCES

Adler, J. 1970 *Combust. Sci. & Tech.* **2**, 105.

Carruthers, J. R. 1976 *J. Crystal Growth* **32**, 13.

Chun, C.-H. & Wuest, W. 1978*a* *Acta Astronautica* **5**, 681.

Chun, C.-H. & Wuest, W. 1978*b* *COSPAR: Space Research* **18**, 523.

Chun, C.-H. & Wuest, W. 1979 *Acta Astronautica* **6**, 1073.

Clark, P. A. & Wilcox, W. R. 1980 *J. Crystal Growth* **50**, 461.

Davis, S. H. & Homsy, G. M. 1980 *J. Fluid Mech.* **98**, 527.

Gumerman, R. J. & Homsy, G. M. 1974 *AIChE J.* **20**, 981.

Kenning, D. B. R. 1968 *Appl. Mech. Rev.* **21**, 1101.

Kölker, H. 1980 *J. Crystal Growth* **50**, 852.

Papazian, J. M., Gutowski, R. & Wilcox, W. R. 1979 *AIAA J.* **17**, 1111.

PEARSON, J. R. A. 1958 *J. Fluid Mech.* **4**, 489.

SCANLON, J. & SEGEL, L. A. 1967 *J. Fluid Mech.* **30**, 149.

SCHWABE, D., SCHARMANN, A., PREISSER, F. & OEDER, R. 1978 *J. Crystal Growth* **43**, 305.

SCHWABE, D. & SCHARMANN, A. 1979 *J. Crystal Growth* **46**, 125.

SCOTT, M. R. & WATTS, H. A. 1975 *Sandia Labs. Rep.* SAND75-0198, *Albuquerque*.

SCOTT, M. R. & WATTS, H. A. 1977 *SIAM J. Num. Anal.* **14**, 40.

SCRIVEN, L. E. & STERNLING, C. V. 1960 *Nature* **187**, 186.

SEN, A. K. & DAVIS, S. H. 1982 *J. Fluid Mech.* **121**, 163.

SIRIGNANO, W. A. 1972 *Combust. Sci. & Tech.* **6**, 95.

SMITH, M. K. 1982 Ph.D. disseration, Northwestern University.

SMITH, M. K. & DAVIS, S. H. 1983 *J. Fluid Mech.* **132**, 145.

SUBRAMANIAN, R. S. 1981 *AIChE J.* **27**, 646.

WILCOX, W. R. 1971 *Preparation and Properties of Solid State Materials* Vol. 1: *Aspects of Crystal Growth*, p. 37. Dekker.

YOUNG, N. O., GOLDSTEIN, J. S. & BLOCK, M. J. 1959 *J. Fluid Mech.* **6**, 350.